**POAC'13**
Espoo, Finland

Proceedings of the 22nd International Conference on
**Port and Ocean Engineering under Arctic Conditions**
**June 9-13, 2013**
**Espoo, Finland**

# AXIALLY SYMMETRIC SOLUTIONS OF SEA ICE DYNAMICS MODELS WITH ELASTIC-PLASTIC AND VISCOUS-PLASTIC RHEOLOGY

Aleksey Marchenko[1,2]
[1]The University Centre in Svalbard, Longyearbyen, Norway
[2]Sustainable Arctic Marine and Coastal Technology (SAMCoT), Centre for Research-based Innovations (CRI), Norwegian University of Science and Technology, Trondheim, Norway

## ABSTRACT
Axially symmetric steady solutions of equations describing ice drift under the influence of cyclonic and anticyclonic wind vortex are constructed and analysed in cases when the ice has elastic-plastic rheology and viscous-plastic rheology. In both cases the solution consists of the ring where the ice is in the plastic state, and the inner kernel and outer ring where the ice stresses are located inside the yield curve. Natural boundary conditions in the origin, at the plastic ring boundaries and on the periphery of the outer ring are formulated. Elastic-plastic solutions satisfying boundary conditions are constructed and analysed in case of cyclonic and anticyclonic wind vortexes. V viscous-plastic solutions have singularity in the origin in case of anticyclonic wind. In case of cyclonic wind the ice thickness grows exponentially at the periphery of the outer ring and the angular velocity of ice drift tends to constant value.

## 1. INTRODUCTION
Modelling of large scale dynamics of drifting ice is based on the consideration of drifting ice rheology at scale of several tens kilometres and greater. Since experiments are not possible at such scale the rheological properties are formulated using intuitive ideas, results of field measurements and analysis of satellite data. Model with elastic-plastic rheology were considered during AIDJEX (see, e.g., Coon et al., 1974), and model with viscous-plastic rheology was formulated by Hibler (1979). Both of the models use normal flow rule with closed yield curve transforming in self-similar manner depending on the ice thickness and compactness. In the elastic-plastic model the ice is considered as an isotropic elastic continuum when the stresses are inside the yield curve. In the viscous-plastic model the ice is modelled as a compressible viscous continuum when the stresses are inside the yield curve.

In the viscous-plastic model the rest is not steady solution of the full set of governing equations including the laws of mass and momentum balance and rheological equations. The reason is related to the pressure existing in rheological equations even when the stresses are located inside the yield curve. The pressure tends to zero for relatively small thickness or compactness of the ice. In the elastic-plastic models the rest performs stationary solution in case when external drag forces and boundary forces are absent. Although the elastic-plastic models look more realistic physically their numerical realisation is more complicated because

of the high speed of elastic waves. Analysis of explicit solutions of the models could demonstrate the difference of modelling results of ice movements in the same conditions when the elastic-plastic and viscous-plastic models are used.

Axially symmetric solutions of equations describing drift of floating ice with elastic-plastic rheology were studied by Schwaegler and Pritchard (1980) numerically for the validation of rheological characteristics of drifting ice in the Arctic and for the investigation of quasi-steady-state response of an axisymmetric ice model driven by a prescribed atmospheric high-pressure system. They determined that the quasi-steady-state response of ice disk with diameter 1000 km is established within six hours of the initial air stress application, regardless of the initial conditions. The study indicated that a purely elastic response occurs for ice strengths approaching the magnitude of 32 kN/m for the conditions considered. Lepparanta (2005) investigated steady axisymmetric solutions of ice drift equations with viscous-plastic rheology for the modelling of zonal ice drift in the Antarctica. The momentum balance equations were performed in spherical coordinates on $\beta$ plane to take into account variations of Coriolis parameter with the longitude. It was shown that rigidly rotating polar cap should exist near the pole to avoid singularity in the ice thickness.

In the present paper axially symmetric and steady solutions including both plastic and elastic regions in the elastic-plastic model and plastic and viscous regions in the viscous-plastic model are constructed and analyzed. In the second section of the paper the statement of the problem, model equations with boundary conditions and main assumptions are formulated. In the third section the stress distribution inside plastic regions of axially symmetric solutions are analyzed. In the fourth and fifth section stress and strain distribution in elastic-plastic and viscous-plastic solutions are discussed. Results of numerical simulations of steady ice drift under cyclonic and anticyclonic wind vortex are performed in the sixth section. Main study results are formulated in the conclusions.

## 2. STATEMENT OF THE PROBLEM, MODEL EQUATIONS AND ASSUMPTIONS

Momentum balance equations describing steady axially symmetric motions of drifting ice are written in the form

$$\frac{d\sigma_{rr}}{dr} + \frac{\sigma_{rr} - \sigma_{\theta\theta}}{r} = \rho_i h A f v_\theta , \qquad (1)$$

$$\frac{d\sigma_{r\theta}}{dr} + \frac{2\sigma_{r\theta}}{r} = -F_\theta , \qquad (2)$$

where $\sigma_{rr}$, $\sigma_{\theta\theta}$ and $\sigma_{r\theta}$ are the components of ice stresses in polar frame of reference $r$ and $\theta$ (positive variations of the angle $\theta$ are in clockwise direction), $v_\theta$ is angular component of ice drift velocity, $\rho_i$ and $h$ are the density and the thickness of the ice cover, $A$ is the ice compactness, $f$ is the Coriolis parameter and $F_\theta$ is the absolute drag force applied to the ice by wind and water. In the Northern Hemisphere the Coriolis parameter $f > 0$. Further the angular velocity $\omega = v_\theta / r$ is used instead $v_\theta$.

It is assumed that radial component of the ice drift velocity equals zero and the equation of mass balance is satisfied explicitly. The ice stresses $\sigma_{rr}$, $\sigma_{\theta\theta}$ and $\sigma_{r\theta}$ are located inside or belong to the yield curve (YC) described by the equation

$$f_Y(\sigma_I, \sigma_{II}, h, A) = 0 , \qquad (3)$$

where $2\sigma_I = \sigma_1 + \sigma_2$, $2\sigma_{II} = \sigma_1 - \sigma_2$, and $\sigma_1$ and $\sigma_2$ are maximal and minimal principal stresses.

Strain rates are calculated from the normal flow rule when the stresses belong to the YC:

$$e_I = \lambda \frac{\partial f_Y}{\partial \sigma_I},\ e_{II} = \lambda \frac{\partial f_Y}{\partial \sigma_{II}},\ \lambda \geq 0, \qquad (4)$$

where $e_I = e_1 + e_2$, $e_{II} = e_1 - e_2$, and $e_1$ and $e_2$ are maximal and minimal principal strain rates. Further we consider solutions family with $\sigma_{rr} = \sigma_{\theta\theta}$. In this case $\sigma_I = \sigma_{rr} = \sigma_{\theta\theta}$ and $\sigma_{II} = |\sigma_{r\theta}|$.

In most of models of sea ice dynamic the YC has a shape of closed curve located in the region of positive pressure ($-\sigma_I \geq 0$) (Fig. 1). Displacement of a part of the YC into the range of positive stresses is associated with the resistance of sea ice cover for the extension or sea ice cohesion. Typically it is assumed that the cohesion is much smaller than yield stresses under the compression. The diameter of the YC depends on the ice thickness and the ice compactness. Normal flow rule (4) sets that plastic deformations are accompanied by an extension ($e_I > 0$) when the pressure is located between the points $O_M$ and $O_C$, and by a compression ($e_I < 0$) when the pressure is located between the points $O_M$ and O (Fig. 1a). The point $O_M$ is associated with the centre of the Mohr circle $M_s$ having tangential point with the YC performed on the Mohr plane $(\sigma_n, \tau_n)$ (Fig. 1b). Pure shear plastic deformations are available only when the stresses are performed by this Mohr circle.

Mapping of the YC from the plane $(\sigma_I, \sigma_{II})$ on the plane $(\sigma_n, \tau_n)$ is available only for those segments of the YC where $|d\sigma_{II} / d\sigma_I| \leq 1$. In this case it is possible to construct the envelope of Mohr circles on the plane $(\sigma_n, \tau_n)$ associated to the points of the YC on the plane $(\sigma_I, \sigma_{II})$. Points of the YC where $|d\sigma_{II} / d\sigma_I| > 1$ are associated with concentric Mohr circles on the plane $(\sigma_n, \tau_n)$. For example, points located on the YC between the points $A_{45}$ and $A_{-45}$ in Fig. 1a) are associated with Mohr circles located inside the Mohr circle $M_{45}$ in Fig. 1b. Mohr circle related to the point O on the plane $(\sigma_I, \sigma_{II})$ in Fig. 1a is shrunk to the point O in Fig. 1b.

The shape of the YC is changed in self-similar way when ice thickness and compactness are varied. Thus the coordinate of the point $O_M$ denoted as $-\sigma_{\max}$, maximal shear stress $\tau_{\max}$ and the coordinate of the point O denoted as $-P$ can be expressed by the formulas

$$\sigma_{\max} = K_\sigma P,\ \tau_{\max} = K_\tau P,\ P = P^* h \exp[-C(1-A)], \qquad (5)$$

where $K_\sigma$ and $K_\tau$ are the coefficients determined by the shape of the YC, and $P^*$ and $C$ are constants.

Further we consider YCI used by Pritchard (1975) and YCII used by Hibler (1979). The YCI and YCII are described by the equations

$$\sigma_{II}^2 = \frac{1}{3}\sigma_I^2\left(1 + \frac{\sigma_I}{P}\right), \text{ (YCI)} \qquad (6)$$

$$\left(\sigma_I + \frac{P}{2}\right)^2 + e^2\sigma_{II}^2 = \frac{P^2}{4}, \text{ (YCII)} \quad (7)$$

$$P^* = 5\,\text{kPa}, \; C = 20, \; e = 2. \quad (8)$$

Coefficients $K_\sigma$ and $K_\tau$ are introduced by the formulas

$$K_\sigma = 2/3, \; K_\tau = 2/9, \text{ (YCI)} \quad (9)$$

$$K_\sigma = 1/2, \; K_\tau = 1/2e, \text{ (YCII)} \quad (10)$$

The upper parts of the YCI and YCII are shown in Fig. 2a when $h = 1\,\text{m}$ and $A = 1$.

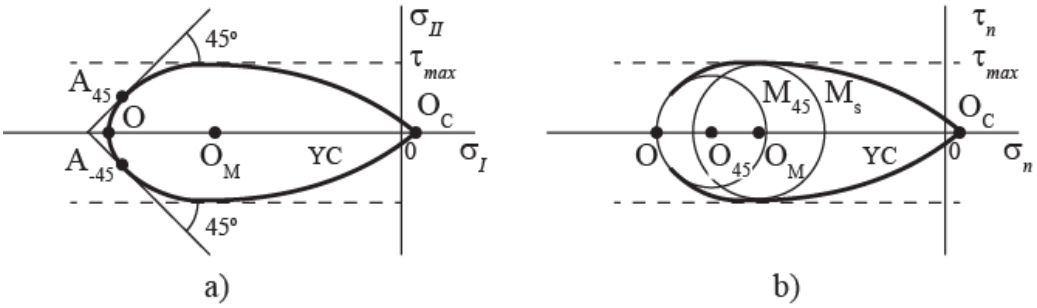


Figure 1**.** Qualitative shape of the Yield curve used in models of sea ice dynamics on the plane $(\sigma_I, \sigma_{II})$ (a) and on the Mohr plane $(\sigma_n, \tau_n)$ (b).

It is assumed that the thickness $h$ of continuous ice can increase only under the ice compression due to the ridging, while the ice extension causes only the decrease of the ice compactness $A$. The compression influences the increase of the ice compactness when $A < 1$. The ice thickness is a constant in two last cases. Thus each of the YC can be performed as a yield surface (YS) in the space $(\sigma_I, \sigma_{II}, h)$ or $(\sigma_I, \sigma_{II}, A)$. Fig. 3 shows the YSI and YSII for the ice with initial thickness $h = 1\,\text{m}$. Each vertical cross-section of the YS by the surface $h = h_0 > 1\,\text{m}$ or $A = A_0 < 1$ performs the the YC of the ice with $h = h_0$ and $A = 1$ or $h = 1\,\text{m}$ and $A = A_0$.

Pure shear deformations of the ice cover are possible when the ice stresses belong to the critical line in the plane $(\sigma_I, h)$ when $A = 1$ or to the critical line in the plane $(\sigma_I, A)$ by $A < 1$. The conception of critical line was introduced by Collins (1990) for wet soils with density dependent yield criteria. The equation of the critical line follows from the condition

$$d\sigma_{II} / d\sigma_I = 0, \quad (11)$$

where the stresses $\sigma_I$ and $\sigma_{II}$ belong to the YS.

The critical lines (CL) of the YSI and YSII are described by the equations

$$\sigma_I = -2P/3, \text{ (CLI)} \quad (12)$$

$$\sigma_I = -P/2. \text{ (CLII)} \quad (13)$$

CLI and CLII are shown in Fig. 2b. It is visible that the CL's almost coincide with the axis $\sigma_I = 0$ when $A < 0.7$. In this case the YC's shrink to the origin at the plane $(\sigma_I, \sigma_{II})$. It means that ice stresses are very small, and the ice cover drifts only under the influence of wind and air drag forces, i.e. the ice drift is free when $A < 0.7$. 3D shape of the Yield surface I is shown in Fig. 3a on the plane $(\sigma_I, h)$ with an extension on the plane $(\sigma_I, A)$.

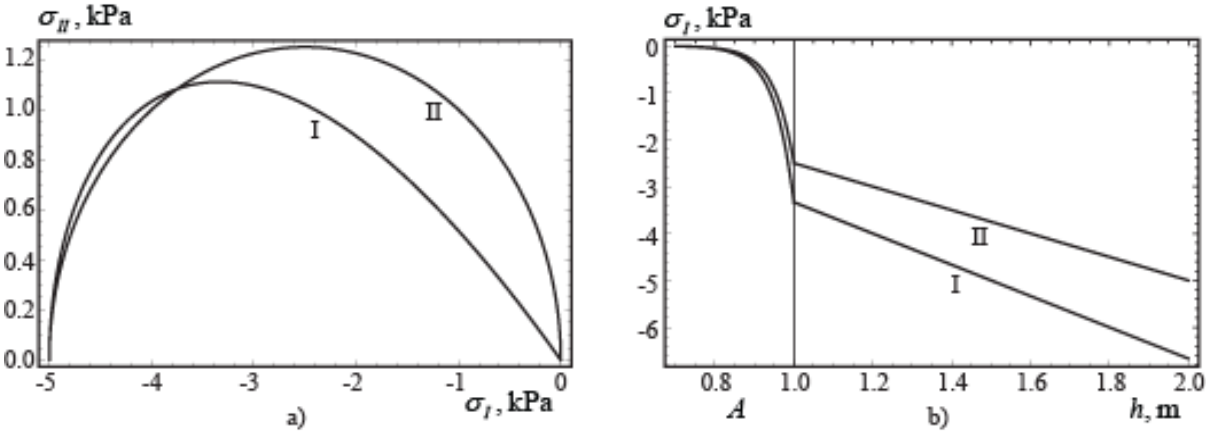


Figure 2. Yield curves I and II (a). Critical lines on the YCI and YCII (b).

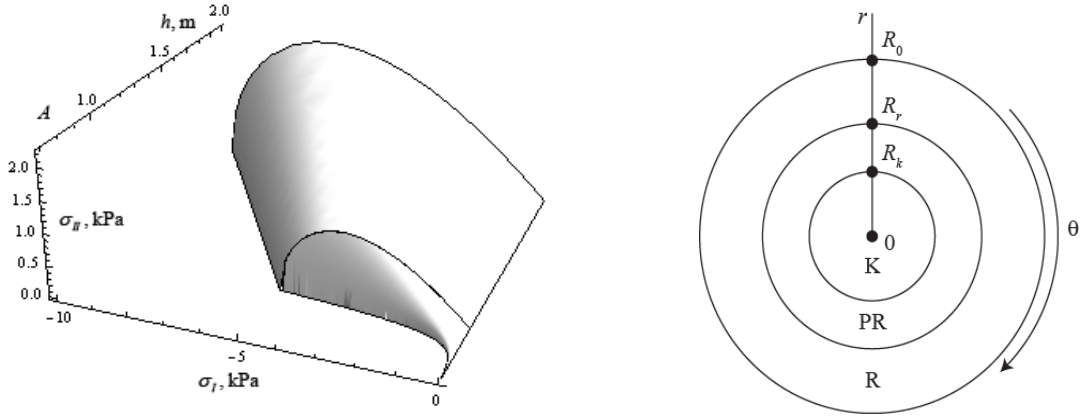


a) b)

**Figure 3**. Yield surface I (a). Configuration of elastic and plastic regions in the steady solution: inner kernel (K), plastic ring (PR) and outer ring (R) (b).

Drag force $F_\theta$ is equal to a sum of wind ($F_a$) and water ($F_w$) drag forces

$$F_a = \delta\rho_a C_a A V_a^2, \quad F_w = -\delta\rho_w C_w A(\omega r)^2, \qquad (14)$$

where $\rho_a$ and $\rho_w$ are air and water densities, $C_a$ and $C_w$ are air-ice and water-ice drag coefficients; $\delta = 1$ for anticyclonic wind vortex ($V_a > 0, \omega \geq 0$), and $\delta = -1$ for cyclonic wind vortex ($V_a < 0, \omega \leq 0$). The angular component of wind velocity $V_a = V_a(r)$ is given as a function of the radius. It is assumed that the function $V_a(r)$ is of the same sign when $r \in (0, L)$, and $V_a(r) = 0$ when $r > L$, where constant $L$ denotes the radius of the wind vortex. Angular velocity $\omega = \omega(r)$ of the ice motion should be found from the solution.

Representative numerical values of physical constants used for estimations are given in Table 1. Values of the drag coefficients $C_w$ and $C_a$ are equal to representative vales used in large scale models of sea ice dynamics (Lepparanta, ). Coriolis parameter $f$ is calculated for the Polar region. It is assumed that representative horizontal scale $L$ is related to typical radius of of the wind vortex, which is about 100 km or greater.

Further we consider a family of steady solutions consisting of the kernel (K) by $r \in (0, R_k)$, the ring with plastic axially symmetric shear flow (PR) by $r \in (R_k, R_r)$ and the outer ring (R)

by $r \in (R_r, R_0)$ where the ice cover is in the rest (Fig. 3b). Inside the PR the angular velocity is a function of the radius $\omega = \omega(r)$ and should be constructed from the solution. In elastic plastic models of drifting ice (Coon eta al, 1974) the kernel K and the ring R are associated with elastic state of the ice. In the viscous-plastic model (Hibler, 1979) the kernel K and the ring R are associated with pure viscous state of the ice. In both cases the ice stresses in the regions K and R are located inside the YS, and the ice stresses in the plastic ring PR belongs to the critical line.

Table 1. Representative numerical values of physical constants

| $\rho_i$, kg/m$^3$ | $\rho_w$, kg/m$^3$ | $\rho_a$, kg/m$^3$ | $C_w$ | $C_a$ | $f$, s$^{-1}$ | $L$, km | $V_a$,m/s | $h$,m | $A$ |
|---|---|---|---|---|---|---|---|---|---|
| 920 | 1020 | 1.27 | 0.005 | 0.002 | $1.454\ 10^{-4}$ | 100 | 10 | 1 | 1 |

Boundary conditions set the continuity of the stresses $\sigma_{rr}$ and $\sigma_{r\theta}$ through the circles $r = R_k$ and $r = R_r$

$$\lim_{r \to R_k - 0} \sigma_{rr} = \lim_{r \to R_k + 0} \sigma_{rr} = -K_\sigma P, \ \lim_{r \to R_k - 0} \sigma_{r\theta} = \lim_{r \to R_k + 0} \sigma_{r\theta} = -\delta K_\tau P, \qquad (15)$$

$$\lim_{r \to R_r - 0} \sigma_{rr} = \lim_{r \to R_r + 0} \sigma_{rr} = -K_\sigma P, \ \lim_{r \to R_r - 0} \sigma_{r\theta} = \lim_{r \to R_r + 0} \sigma_{r\theta} = -\delta K_\tau P. \qquad (16)$$

Since the ice in the origin is not confined it is assumed that

$$\lim_{r -> 0} \sigma_{r\theta} = 0. \qquad (17)$$

## 3. STRESSES IN THE PLASTIC RING

The ice motion in the PR is performed by pure shear deformations, when $e_I = 0$ and $\partial f_Y / \partial \sigma_I = 0$. The second formula (4) is used for the finding of the coefficient $\lambda$ which should not be negative. In this solution the angle between slip lines is equal to 90$^o$. The first family of slip lines coincides with concentric circles and the second family is performed by radial lines; $\sigma_{rr} = \sigma_{\theta\theta}$ since normal stresses should be the same on both slip lines passing through the same point.

In the PR the stresses belong to the Mohr circle $M_s$ (Fig. 1b) and expressed as follows

$$\sigma_{rr} = \sigma_{\theta\theta} = -K_\sigma P, \ \sigma_{r\theta} = -\delta K_\tau P, \ r \in (R_k, R_r). \qquad (18)$$

Substituting formulas (19) into equations (1) and (2) we find

$$K_\sigma dP / dr = -\rho_i h A f \omega r, \qquad (19)$$

$$K_\tau dP / dr + 2K_\tau P / r = \delta F_\theta. \qquad (20)$$

From equations (19) and (20) the angular velocity is expressed as follows

$$\omega r = \frac{\rho_i h A f K_\tau K_\sigma^{-1} + \delta \sqrt{\Delta}}{2\rho_w C_w}, \ \Delta = \left(\rho_i h A f K_\tau K_\sigma^{-1}\right)^2 + \rho_w C_w \left(\rho_a C_a V_a^2 - \frac{2K_\tau P}{r}\right). \qquad (21)$$

Using values from formulas (8)-(10) and Table 1 we find estimates

$$\rho_w \rho_a C_w C_a V_a^2 \approx 1.3\,\mathrm{kg^2/(m^4 s^2)}, \qquad (22)$$

$$\left(\rho_i h A f K_\tau K_\sigma^{-1}\right)^2 \approx 0.0018\,\mathrm{kg^2/(m^4 s^2)}, \ 2\rho_w C_w K_\tau P L^{-1} \approx 0.11\,\mathrm{kg^2/(m^4 s^2)}, \text{ (YCI)} \qquad (23)$$

$$\left(\rho_i h A f K_\tau K_\sigma^{-1}\right)^2 \approx 0.004\,\mathrm{kg^2/(m^4 s^2)}, \ 2\rho_w C_w K_\tau P L^{-1} \approx 0.13\,\mathrm{kg^2/(m^4 s^2)}. \text{ (YCII)} \qquad (24)$$

Therefore $\Delta \approx \rho_w C_w \rho_a C_a V_a^2$ with accuracy to high order terms in range where the wind velocity is about 10 m/s. In formula (21) the sign "+" in front of term $\delta\sqrt{\Delta}$ should be used

since the wind velocity and the velocity of ice drift should have the same direction. As a result solution (21) can be approximated by the formula

$$\omega r \approx 0.5\delta V_a \sqrt{\rho_a C_a /(\rho_w C_w)}\,. \qquad (25)$$

Thus maximal ice drift speed in the PR is smaller in two times the free drift velocity estimated from the balance of the drag forces $F_a + F_w = 0$.

From the second formula (22) follows that the determinant $\Delta$ is positive when

$$V_a^2 > V_{cr}^2,\ \ V_{cr}^2 = \left(2\rho_w C_w K_\tau Pr^{-1} - \left(\rho_i hAfK_\tau K_\sigma^{-1}\right)^2\right)(\rho_w C_w \rho_a C_a)^{-1}. \qquad (26)$$

Estimates (23) and (24) show that condition (26) can be satisfied in the range $r \in (r_1, r_2)$ when wind velocity $V_a$ is finite in the vicinity of the origin and by $r > L$. In this range condition $V_{cr}^2 > 0$ is satisfied, and the plastic ring boundaries $r = R_k$ and $r = R_r$ belong to this range as well. The angular velocity $\omega$ should be positive in case of anticyclonic wind vortex ($\delta = 1$) and negative in case of cyclonic wind vortex ($\delta = -1$).

Integration of equation (20) with $A = 1$ and using formula (25) leads to the formula

$$h = h_0 \exp[-\delta K_h \int_{r_0}^{r} V_a dr],\ \ K_h = \frac{\rho_i f}{2\beta K_\sigma}\sqrt{\frac{\rho_a C_a}{\rho_w C_w}}\,, \qquad (27)$$

where $h = h_0$ by $r = R_k$. Integration of equation (20) from $A = 1$ to $A < 1$ with $h = const$ leads to the formula

$$F_A(A) = -\delta K_A \int_{r_1}^{r} V_a dr\,,\ \ F_A(A) = \int_1^A \exp[-C(1-t)]/t\, dt\,, \qquad (28)$$

where $A = 1$ by $r = r_1$ and $K_A = K_h / C$.

From formula (28) follows that the ice thickness $h$ and the ice compactness $A$ increase with the decreasing of radius $r$ in anticyclonic wind vortex. In cyclonic wind vortex the situation is opposite. Function $F_A(A) \approx -0.06$ when $A < 0.7$. In this range very small changes of the integral from the wind velocity in (28) can cause fast drop of the ice compactness to zero. Formula (21) shows that the angular velocity $\omega$ can be equal to zero inside the range where $\Delta > 0$ when $\delta < 0$ (cyclonic wind), and it is always greater zero inside the range where $\Delta > 0$ when $\delta > 0$ (cyclonic wind). It explains further described effect of the transformation of elastic-plastic solution with rotating elastic kernel to pure elastic solution with rotating elastic kernel and plastic ring of zero thickness when maximal wind speed drops to a critical.

## 4. STRESSES IN THE ELASTIC-PLASTIC SOLUTION

The elastic kernel rotates with constant angular velocity $\omega_{ek}$. Ice stresses inside the elastic kernel can be performed as a sum of the stresses expressed through the stress function

$$U = A_1\theta + A_0 r^2 \ln r + B_0 r^2 + C_0 \ln r\,, \qquad (29)$$

and the stresses accounting the drag forces. Constants $A_0$ and $C_0$ are equal to zero since the stresses are limited at the origin. Constants $A_1$ and $B_0$ are found from the boundary conditions (15) and (17). Finally the stresses are expressed as follows

$$\sigma_{rr} = \sigma_{\theta\theta} = -K_\sigma P_{ek} + \rho_i f \omega_{ek} \int_{R_{ek}}^{r} hAr dr\,,\ r \in (0, R_{ek}), \qquad (30)$$

$$\sigma_{r\theta} = -\delta\rho_a C_a f_{ek}(r) + \delta\rho_w C_w \omega_{ek}^2 g_{ek}(r)\,,\ \ r \in (0, R_{ek}), \qquad (31)$$

where $P_{ek}$ is the value of $P$ at $r = R_{ek}$. Functions $f_{ek}(r)$ and $g_{ek}(r)$ are calculated with the formulas

$$f_{ek}(r) = f(0, r),\ g_{ek}(r) = r^{-2}\int_0^r Ar^4 dr, \tag{32}$$

$$f(r_1, r_2) = r^{-2}\int_{r_1}^{r_2} AV_a^2 r^2 dr. \tag{33}$$

The ice drift velocity is equal to zero inside the elastic ring, and the ice stresses are expressed by the formulas

$$\sigma_{rr} = \sigma_{\theta\theta} = -K_\sigma P_{er},\ r \in (R_{er}, R_0), \tag{34}$$

$$\sigma_{r\theta} = -\delta f_{er}(r) - \delta K_\tau P_{er} R_{er}^2 / r^2,\ \ r \in (R_{er}, R_0), \tag{35}$$

where $P_{er}$ is the value of $P$ at $r = R_{er}$ and $f_{er}(r) = f(R_{pr}, r)$. Substituting formula (31) into the second boundary condition (15) we find formula for the calculation of inner radius of the plastic ring $R_{ek}$

$$\rho_a C_a f_{ek}(R_{ek}) - \rho_w C_w \omega_{ek}^2 g_{ek}(R_{ek}) = K_\tau P_{ek}. \tag{36}$$

## 4. STRESSES IN VISCOUS-PLASTIC SOLUTION

In the viscous kernel and viscous ring the radial velocity of the ice drift is equal zero, and angular velocity $\omega$ depends on the radius $r$. Therefore strain rates are determined according to the formulas

$$\dot{\varepsilon}_{rr} = 0,\ \dot{\varepsilon}_{\theta\theta} = 0,\ \dot{\varepsilon}_{r\theta} = \frac{r}{2}\frac{d\omega}{dr}. \tag{37}$$

Hibler's (1979) viscous stresses in the ice are expressed by the formulas

$$\sigma_{rr} = \sigma_{\theta\theta} = -P/2,\ \sigma_{r\theta} = \eta P r \frac{d\omega}{dr}, \tag{38}$$

where $\eta = 2.5 \cdot 10^8$ s. Substituting formulas (38) in equations (1) and (2) we find

$$dP/dr = -2\rho_i h A f \omega r, \tag{39}$$

$$\eta r d\left(P d\omega/dr\right)/dr + 3\eta P d\omega/dr = -F_\theta. \tag{40}$$

Equations (40) and (41) determine variations of $\omega$ and $P$ inside the viscous kernel by $r \in (0, R_{vk})$ and inside the viscous ring $r \in (R_{vr}, R_0)$.

At the boundary between the viscous kernel and the plastic ring normal stress $\sigma_{rr}$ and shear stress $\sigma_{r\theta}$ should be continuous

$$\lim_{r \to R_{vk}-0} P = \lim_{r \to R_{vk}+0} P,\ \lim_{r \to R_{vk}-0} \eta r d\omega/dr = -\delta K_\tau \tag{41}$$

Similar conditions are valid at the boundary between the plastic ring and the viscous ring

$$\lim_{r \to R_{vr}-0} P = \lim_{r \to R_{vr}+0} P,\ \lim_{r \to R_{vr}+0} \eta r d\omega/dr = -\delta K_\tau. \tag{42}$$

Conditions (41) and (42) set up the continuity of the ice thickness or the ice compactness in the points $r = R_{vk}$ and $r = R_{vr}$.

It is assumed that the angular velocity is finite at the origin and continuous at the boundary between the viscous kernel and the plastic ring

$$|\omega| < \infty,\ r \to 0,\ \lim_{r \to R_{vk}-0} \omega = \lim_{r \to R_{vk}+0} \omega \tag{43}$$

Second condition (43) means that the angular velocity at the boundary between the viscous kernel and the plastic ring satisfies formula (21). The angular velocity is zero at the outer boundary of the viscous ring

$$\lim_{r \to R_0} \omega = 0 . \qquad (44)$$

Substituting the expression of $dP/dr$ from equation (39) into equation (40) we find

$$rPd^2\omega/dr^2 + \left(3P - 2\rho_i fhA\omega r^2\right)d\omega/dr = -\eta^{-1}F_\theta . \qquad (45)$$

Near the origin and at the periphery of the viscous ring the wind velocity is small and the right part of equation (45) is approximated by the formula $F_\theta \approx F_w$, where the water drag force $F_w$ is determined by formula (14).

Numerical analysis of equations (39) and (40) combined with the analysis of equation (45) by $A = 1$ shows that in anticyclonic wind the solution has the following asymptotic in the origin

$$h \to const,\ r\omega \to \infty,\ r^2\omega \to 0,\ rd\omega/dr \to -\infty,\ r \to 0 . \qquad (46)$$

Therefore the first boundary condition (43) is not satisfied and the viscous kernel can't be extended to the origin. In case of cyclonic wind the solution at the periphery of the viscous kernel has asymptotic

$$\omega = \omega_0 + \omega'_0\, e^{-\alpha r^2},\ h = h_0 e^{\alpha r^2},\ \alpha = \rho_i f\omega_0 / P^* , \qquad (47)$$

where constants $\omega_0 < 0$, $\omega'_0 < 0$ and $h_0 > 0$ are determined by the solution inside the plastic ring. Therefore boundary condition (44) is not satisfied at the outer boundary of the viscous ring.

## 6. RESULTS OF NUMERICAL SIMULATIONS

Numerical simulations were performed with $A = 1$ and wind velocity

$$V_a = 4V_{\max}\frac{r^2}{L^2}\left(1 - \frac{r^2}{L^2}\right),\ r \in (0, L);\ V_a = 0,\ r > L , \qquad (48)$$

where $L$ is the radius of the wind vortex, and $V_{\max}$ is the maximal wind velocity in the vortex.

Substitution of formula (48) into (33) leads to the formula

$$f(0,r) = 16V_{\max}^2\frac{r^5}{L^4}\left(\frac{1}{7} - \frac{2r^2}{9L^2} + \frac{r^4}{11L^4}\right),\ r \in (0, L);\ f(0,r) = \frac{f(0,L)L^2}{r^2},\ r > L , \qquad (49)$$

where $f(0, L) \approx 0.185 \cdot V_{\max}^2$.

Pure elastic solution of the problem exists when $\omega_e = 0$ and maximal shear stress $\sigma_{II}$ is located inside the YK. Compressive stress $\sigma_I$ satisfies to the condition $3\rho_a^2 C_a^2 f_{\max}^2 < \sigma_I^2\left(1 + \sigma_I / P\right)$. Thus shear motion of the ice cover is absent when $\rho_a C_a f_{\max} < K_\tau P$, and develops when $\rho_a C_a f_{\max} > K_\tau P$. Conditions for the limit equilibrium $\rho_a C_a f_{\max} = K_\tau P$ are formulated as follows

$$\rho_a C_a f_{ek}(r) = K_\tau P,\ df_{ek}(r)/dr = 0 . \qquad (50)$$

Numerical solution of equations (50) gives the estimate

$$r = r_{cr} \approx 0.88L,\ |V_{\max}| = V_{cr} = \sqrt{4.76PK_\tau/(\rho_a C_a L)} . \qquad (51)$$

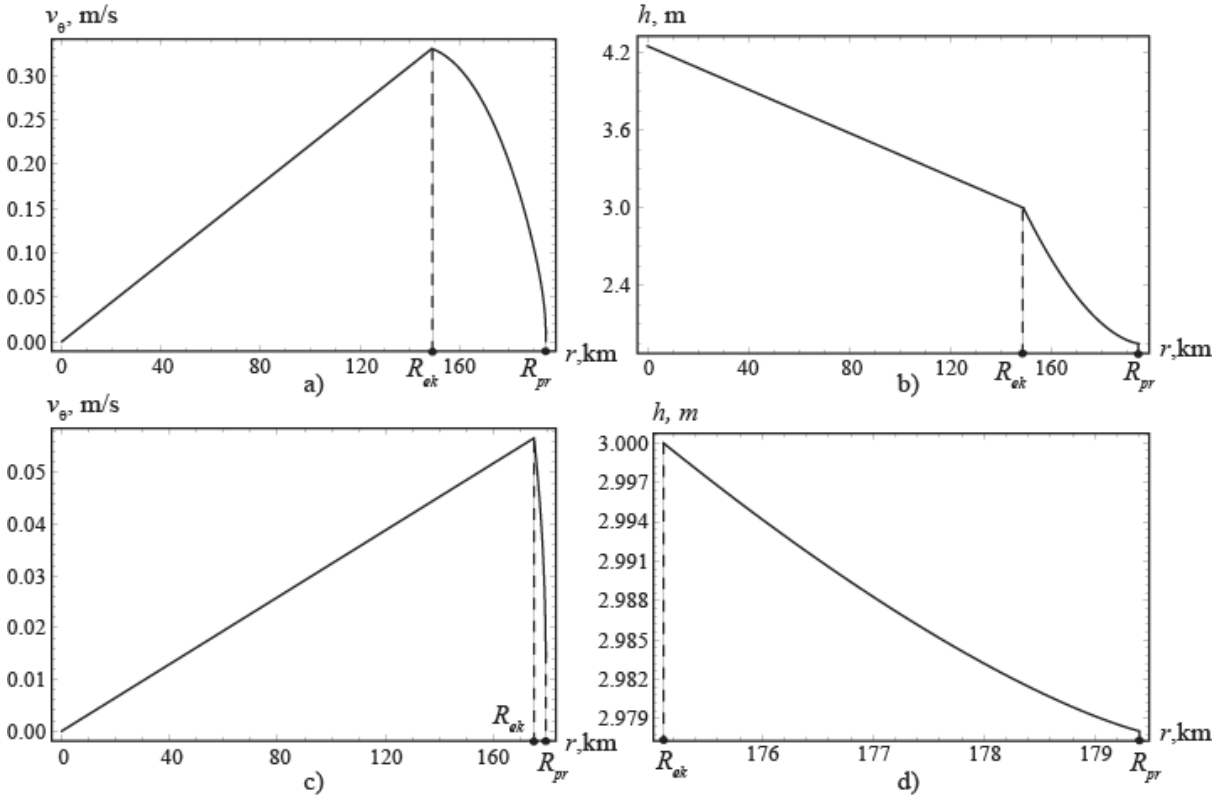


Figure 4. Radial distribution of the ice velocity $v_\theta$ (a,c) and the ice thickness (b,d) in anticyclonic ice vortex constructed with maximal wind velocity $V_{\max} = 15\,\text{m/s}$ (a,b) and $V_{\max} = 6\,\text{m/s}$ (c,d). Radius of the wind vortex is $L = 200\,\text{km}$ and the ice thickness $h_{pr,ek} = 3\,\text{m}$.

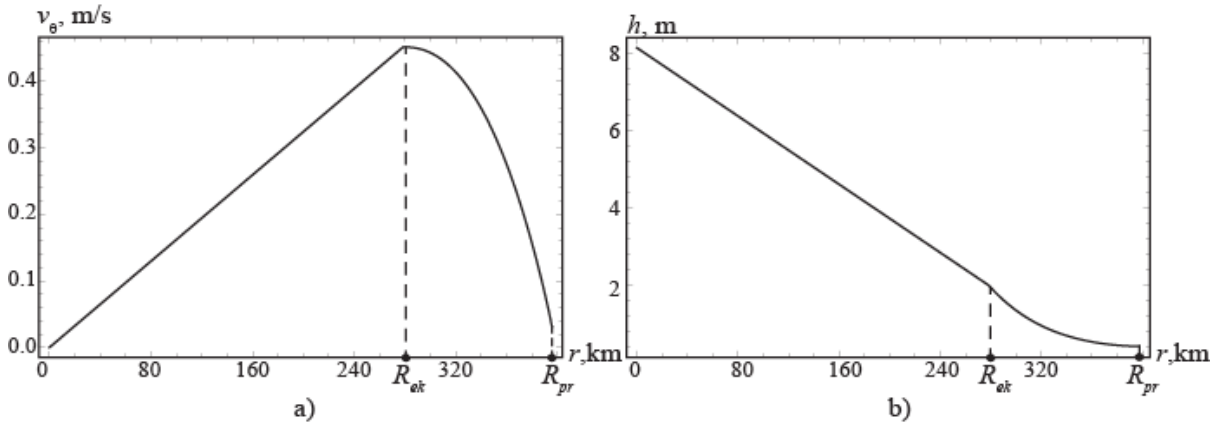


Figure 5. Radial distribution of the ice velocity $v_\theta$ (a) and the ice thickness (b) in anticyclonic ice vortex constructed with maximal wind velocity $V_{\max} = 20\,\text{m/s}$, the radius of the wind vortex $L = 400\,\text{km}$ and the ice thickness $h_{pr,ek} = 2\,\text{m}$.

Graphs in Fig. 4 are constructed with the anticyclonic wind vortex of the radius $L = 200\,\text{km}$ and the ice thickness $h_{pr,ek} = 3\,\text{m}$. Graphs in Fig. 4a,b and Fig. 4c,d are constructed with $V_{\max} = 15\,\text{m/s}$ and $V_{\max} = 6\,\text{m/s}$ respectively. One can see that the angular velocity of the anticyclonic ice vortex tends to different from zero value when $V_{\max}$ decreases, and there is discontinuity of ice drift velocity at $r = R_{pr}$. The dependence of the ice thickness from the polar radius inside the elastic kernel is not unique. Fig. 4b shows linear distribution

of ice thickness over the elastic kernel. The stresses inside the elastic kernel are inside the Yield curve (6). In Fig. 4d the ice thickness is equal to $h_{pr,er}$ inside the elastic kernel. From Fig. 8b follows that the ice thickness in the origin exceeds the ice thickness at the boundary of the elastic kernel due to the Coriolis force action. Fig. 4c shows the existence of discontinuity in the drift velocity at the outer boundary of the plastic ring by $r = R_{pr}$. Figure 5 shows the characteristics of anticyclonic ice vortex constructed for the wind vortex with $V_{\max} = 20\,\text{m/s}$, $L = 400\,\text{km}$ and ice thickness $h_{pr,ek} = 2\,\text{m}$. The width of the plastic ring reaches 119.19 km. Fig. 5a shows the existence of discontinuity in the drift velocity at the outer boundary of the plastic ring by $r = R_{pr}$. Fig. 5b demonstrates significant drop of the ice thickness over the PR from $h_{pr,ek} = 2\,\text{m}$ at $r = R_{ek}$ to $h_{pr,er} = 42\,\text{cm}$ at $r = R_{pr}$. Since the ice thickness can not drop below the thickness of ice formed by thermal growth (1.5-2 m) this effect should be reformulated by the reduction of the ice compactness. It could explain the lead opening at the periphery of the anticyclonic vortex. Fig. 5b demonstrates significant increase of the ice thickness in the origin due to the Coriolis force action.

## 7. CONCLUSIONS

Equations describing axially symmetric motion of the ice cover with elastic-plastic rheologyand viscous-plastic rheology were formulated. Axially symmetric solutions of the equations were constructed and analysed in cases when the ice drift is exited by cyclonic or anticyclonic wind vortex. All constructed solutions include the plastic ring with pure shear motions of the ice. In the elastic-plastic solutions the plastic ring is located between the inner elastic kernel and outer elastic ring. Natural boundary conditions are satisfied in the origin and at the periphery of the elastic ring. In the viscous-plastic solutions the plastic ring is located between the inner kernel and outer ring with pure viscous state of the ice. In case of anticyclonic drift the drift velocity has singularity in the origin, and in case of cyclonic drift the angular drift velocity tends to a constant with the increase of the radius of the viscous ring. The ice thickness increases exponentially with the increase of the radius of the viscous ring in case of cyclonic ice drift. The influence of the Coriolis force influences the increase of the ice thickness from the periphery of the plastic ring to the elastic kernel in anticyclonic ice vortex. The ice thickness in the plastic ring is changed in opposite direction in case of cyclonic ice vortex. This effect can influence the lead opening in case of anticyclonic wind vortex and the ice ridges buildup in case of cyclonic wind vortex at the periphery of the plastic ring.

## REFERENCES


Collins, I.F., 1990. Plane strain characteristic theory for soils and granular materialswith density dependent yield criteria. J. Mech. Phys. Solid., 38 (1), pp. 1-25.

Coon, M.D., Maykut, G.A., Pritchard, R.S., Rothrock, D.A., and Thorndike, A.S., 1974. Modeling
the pack ice as an elastic-plastic material. AIDJEX Bull. 24, pp. 1–105.

Hibler, W.D. III, 1979. A dynamic thermodynamic sea ice model. J. Phys. Oceanogr.
9, pp. 815–846

Lepparanta, M., 2005. The drift of sea ice. Praxis Publishing Ltd, Chichester, UK, 266 p.

Pritchard, R.S., 1975. An elastic-plastic constitutive law for sea ice. J. Appl. Mech. 42E, pp. 379–384.

Schwaegler, R.T., and Pritchard, R.S., 1980. AIDJEX model response to axisymmetric loadings. Proc. of the AUDJEX. International Commission on Snow and Ice Symposium. Pritchard (ed.), University of Washington Press, Seattle and London, pp. 134-139.